LETTER

Contiguous Petal-like Carbon Nanosheet Outgrowths from Graphite Fibers by Plasma CVD

Thiruvelu Bhuvana,[†] Anurag Kumar,[†] Aditya Sood,[†,‡] Roger H. Gerzeski,[§] Jianjun Hu,[§] Venkata Srinu Bhadram,[||] Chandrabhas Narayana,[||] and Timothy S. Fisher*[,†,§]

Birck Nanotechnology Center, Purdue University, West Lafayette, Indiana 47907, Department of Materials and Metallurgical Engineering, Indian Institute of Technology, Kanpur 208016, India, Air Force Research Laboratory, Thermal Sciences and Materials Branch (AFRL/RXBT), 2941 Hobson Way, Wright-Patterson AFB, Ohio 45433-7750, and Chemistry and Physics of Materials Unit, Jawaharlal Nehru Centre for Advanced Scientific Research, Jakkur P. O., Bangalore 560064, India

ABSTRACT We report a catalyst-free synthesis of cantilevered carbon nanosheet extensions, or petals, from graphite fibers by microwave plasma CVD. Results reveal that the petals grow from the fiber surface layers while preserving graphitic continuity from fiber to the petals. Subtraction of Raman signatures from pristine and decorated fibers reveals a convolution of two underlying peaks at 2687 and 2727 cm^{-1} that are consistent with profiles of multilayer graphene flakes between 5 and 25 layers. Such structures offer the possibility of minimizing interfacial losses in transport applications, improved interactions with surrounding matrix materials in composites, and a route toward substrate independence for device applications.

KEYWORDS: carbon fiber • fiber composite • graphene • graphite flake • carbon nanosheet

INTRODUCTION

Spatially confined forms of crystalline carbon materials (e.g., carbon nanotubes, graphene) possess unique and intriguing electronic, mechanical, thermal, and chemical properties (1, 2). To serve useful functions, these materials must be connected to larger-scale elements, and often, these mesoscopic interfaces become the critical factors in the performance of these materials. For example, the behavior of carbon nanotube transistors is largely dictated by their metallic source and drain contacts (3). Similarly, thermal resistance across carbon nanotube arrays is dominated by their interfaces to bulk elements (4, 5), and the efficacy of carbon nanotube additives for structural reinforcement of composites has been shown to be limited by their poor interactions with surrounding matrix resins (6). Graphene has recently received attention as a promising composite additive (7, 8) and as an electronic device element (9, 10), in part because its electronic structure is less sensitive to lattice orientation as compared to single-walled carbon nanotubes, which require a high degree of chirality control (3). However, the electronic structure of graphene can be strongly influenced by substrate interactions (11, 12), which ideally would be avoided through the creation of suspended graphene structures. In this paper, we report a graphene synthesis approach that addresses the issues of edge interconnection and substrate interactions through the synthesis of cantilevered multilayer graphene sheet- or petal-like outgrowths that are seeded from a core graphite fiber. The resulting structures offer the possibility of minimizing interfacial losses in transport applications, improved interactions with surrounding matrix materials in composites, and a route toward substrate independence for device applications.

Plasma-enhanced chemical vapor deposition (PECVD) has been widely used for the growth of different carbon nanostructures such as carbon nanotubes (13), carbon nanosheets (12, 14, 15), and diamond films (16). Microwave plasma CVD (MPCVD) was recently used to grow vertically oriented graphene on a variety of substrates (17), and graphite flakes have been deposited on the walls of a stainless steel microwave MPCVD chamber (18). DC arc discharge of graphitic electrodes has also been shown to yield petal-like graphite sheets (19). Mixtures of H_2 and He suitably proportioned in an arc discharge can also be used to improve graphene growth (20), with the hypothesis that H_2 serves to terminate the dangling bonds in the evaporated graphite thereby preventing it to form closed structures such as CNTs.

The main advantage of the method discussed in the present paper, apart from not requiring metal catalysts to drive growth, is that heterojunctions do not exist between graphene and the underlying substrate-in this case a graphite fiber. In prior work, carbon nanotubes have been used in conjunction with graphite fibers to improve mechanical composite properties (21), and carbon nanosheets without fibers have been shown to enhance the thermal properties

* Corresponding author. E-mail: timothy.fisher@wpafb.af.mil.
Received for review December 22, 2009 and accepted February 9, 2010
[†] Purdue University.
[‡] Indian Institute of Technology.
[§] Air Force Research Laboratory.
[||] Jawaharlal Nehru Centre for Advanced Scientific Research.
DOI: 10.1021/am9009154

Published on Web 02/16/2010

of epoxies substantially (22). In the present work, the fiber substrate itself provides sites for nucleation of the graphite petals. This type of contiguous monolithic growth is expected to lead to a significant improvement in mechanical and transport properties of the fibers when used in composite or device applications. Homojunctions avoid internal stresses arising from the mismatch of lattice parameters and formation of intermediate amorphous or carbide phases (23), such that weak bonds and interfacial resistances do not form. For example, such petal-decorated fibers are expected to improve the strength and integrity of interfaces between the fiber and polymer matrix in bulk composites (6).

Many different forms of graphite fibers exist and are commonly used as strengthening agents in composites (24). Highly graphitized fibers, such as Cytec's P100, made from melt-spun liquid crystal mesophase pitch (25) exhibit numerous desirable mechanical, electrical and thermal properties. They are exceptionally stiff (high tensile and compressive modulus), usefully strong (moderate tensile and compression strength), and have moderately to very high electrical and thermal conductivities (26). Unfortunately, their structure consisting of stacked multiple crystals of graphite basal planes (27, 28) render them unable to transfer these desirable properties from fiber to fiber (29). Highly graphitic fibers, such as P100, primarily present the normal to the graphite basal planes on their surfaces (27, 29). Because chemical modification and functionalization of the basal planes is almost impossible, use of the fibers in a bulk composite results in poor effective material properties (27). Numerous attempts to modify the surfaces of graphite fibers by chemical and plasma means have resulted in modest success (29, 30). One relatively promising approach involves the use of oxygen plasma (29), which removes folded graphite basal planes at the fiber surface and implants oxygenated groups. This approach moderately improves the mechanical properties of composites using graphite fibers, but it has not been shown to improve thermal or electrical properties.

RESULTS AND DISCUSSION

P100 graphite fibers of 10 μm diameter elevated 6 mm above a Mo puck were subjected to MPCVD conditions of H_2 (50 sccm) and CH_4 (10 sccm) as the primary feed gases at 30 Torr total pressure and 700 W plasma power; further details of the synthesis process are provided as Supporting Information. Figure 1 contains several SEM images of carbon fibers. In Figure 1a, which corresponds to 10 min growth duration, petal-like outgrowths are clearly apparent, and the predominant two-dimensional orientation appears to lie in the plane normal to the fiber surface and oriented along the fiber's axis. The inset of Figure 1a shows a pristine carbon fiber without any pretreatment to illustrate the relatively smooth surface of the fiber before growth.

Figure 1b corresponds to 30 min of growth time and illustrates the continued growth of the petals, which retain a general orientation along the fiber's axis. The petals have grown approximately 500 nm out from the surface, and the typical span width of a single unwrinkled two-dimensional

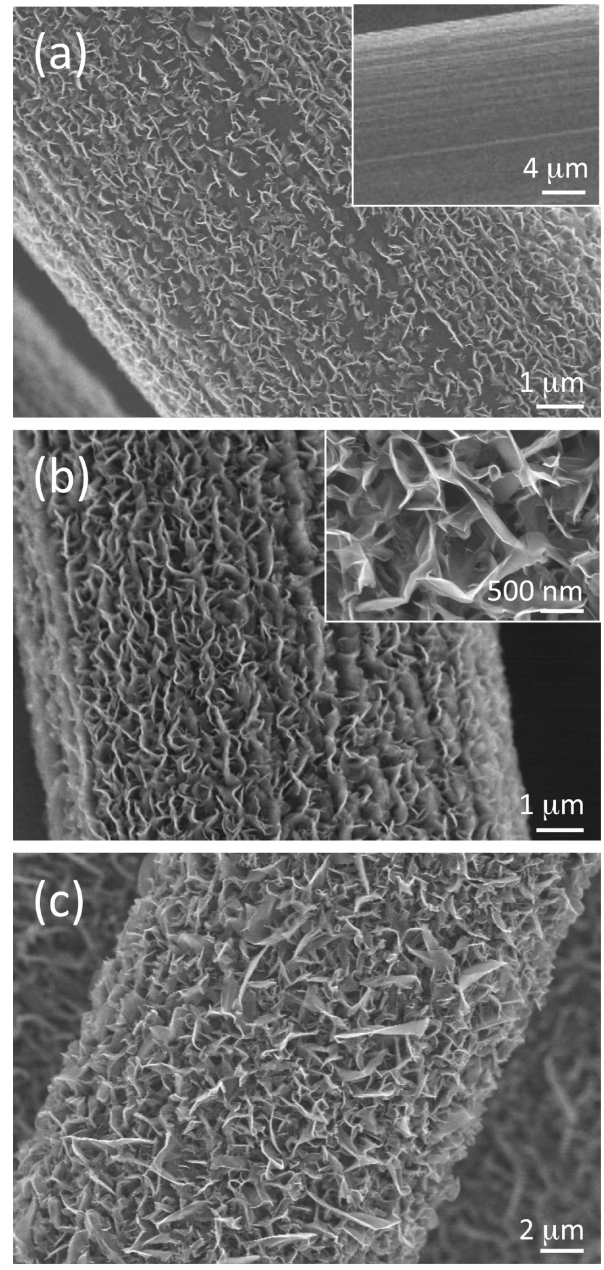

FIGURE 1. SEM images of the graphene outgrowth on carbon fiber carried out for different growth durations in the presence of oxygen: (a) 10 min with inset showing pristine fiber and (b) 30 min with inset showing a magnified image. (c) Growth without oxygen for 30 min.

grain is approximately 250−1000 nm (see inset in Figure 1b). Further, the growth appears to be of microscopically uniform density both axially and circumferentially. Figure 1c shows the growth carried out in the absence of oxygen. Though uniform growth occurs, the petals are less oriented to the fiber axis and appear to be thicker.

We note that elevation of the fibers above the Mo puck was found to be essential to the growth process, as placement of fibers directly on the puck surface resulted in no significant growth. This elevation resulted in a marked increase in the intensity of visible thermal radiation from the fiber surface. Presumably, the enhanced electric field near the elevated fibers results in an increased flux of plasma

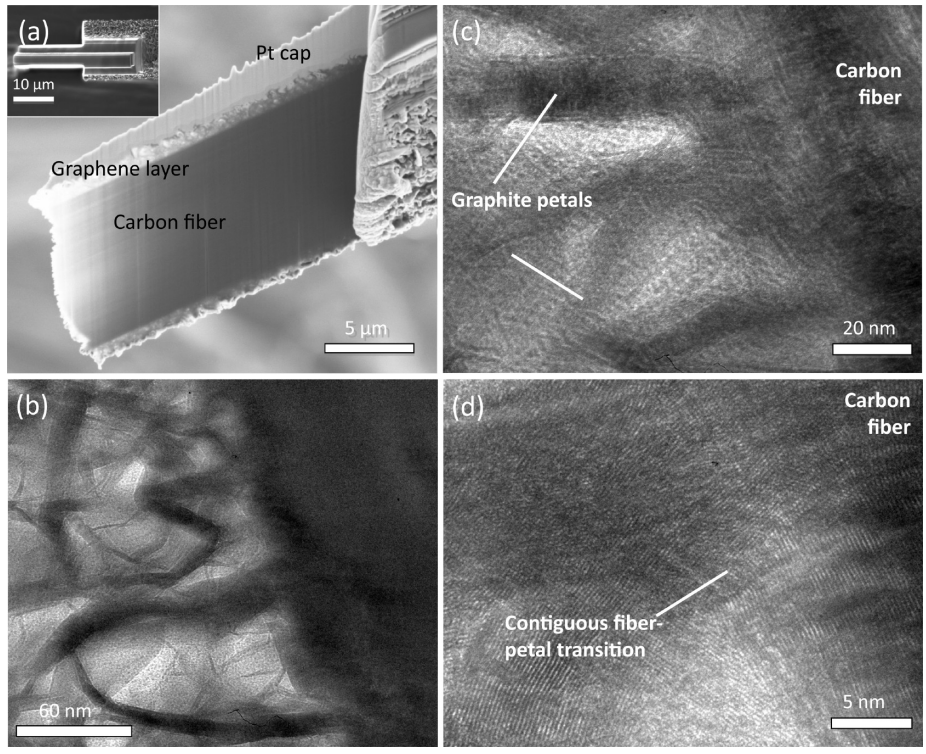

FIGURE 2. Electron microscope images of (a) the cross-sectional microstructure of petal-decorated graphite fibers by SEM, (b) low-resolution TEM images showing petals of 5−15 nm in width, (c) and (d) magnified TEM images of the fiber/petal interface showing neither significant disruption to the atomic arrangement of petal layers nor disordered amorphous regions at the interface.

radicals. Such influx would increase fiber temperature. Based on measurements recorded by a dual-wavelength pyrometer (Williamson PRO 92), the fiber temperature during growth is estimated to be approximately 1650 K as detailed in the Supporting Information. The likely mechanism of petal growth involves deposition of hydrocarbon radicals at or near the exposed surface graphene edges, which may be accentuated by the hydrogen−oxygen plasma pretreatment. According to Petherbridge et al. (31) and supported by recent work by Garg et al. (32), the critical factor in determining the preference for diamond sp^3 lattice structures or graphene sp^2 structures upon deposition is the ratio of atomic hydrogen to acetylene in the plasma mixture. The present deposition pressure and plasma power conditions are similar to those that produce diamond growth (33), but the gas composition is more similar to that for carbon nanotube growth (13) and is expected to be the most significant factor in determining the hydrogen:acetylene ratio. Further elucidation of the growth mechanism will require detailed plasma diagnostics experiments, which are ongoing.

A focused ion beam (FIB) microscope was employed to prepare the TEM specimens in order to analyze the cross-sectional microstructure of petal-decorated graphite fibers, as shown in Figure 2a. To protect the fiber surfaces from bombardment, we deposited a Pt protection cap of 2 μm thickness on the top surface using a gas injection system under e-beam irradiation. Well-aligned graphite layers of 0.34 nm spacing were revealed in the graphite fiber parallel to its axis direction, indicating that the original fiber microstructure was preserved during MPCVD growth. The petal outgrowths appear to be 5−15 nm in width (see Figure 2b), representing up to dozens of graphene layers. Neither significant disruption to the atomic arrangement of graphite layers nor disordered amorphous regions are apparent in the fiber/petal interface. Therefore, the growth mechanism appears to involve sprouting and branching of petals from the superficial graphite fiber surface layers while maintaining the continuity of graphite structure from the fiber to petals (see Figure 2c,d).

Raman spectra of (i) a pristine carbon fiber and (ii) a carbon fiber with a petal-decorated surface recorded in a backscattering arrangement, under 532 nm laser excitation at 8 mW power (34), are shown in Figure 3a. Raman spectroscopy gives rich microscopic information of the various all-carbon allotropes. In the case of graphitic carbon, Raman spectra present several characteristic bands: a G band near 1580 cm^{-1}, a D band near 1350 cm^{-1}, a 2D band near 2700 cm^{-1}, and a weak D′ feature near 1620 cm^{-1} and its 2D′ overtone near 3240 cm^{-1}. Though first-order Raman processes look at only the Brillouin Zone (BZ) center phonons, the D band has been associated with defect-mediated phonons near the BZ edge (near K-point), and a finite 2D band intensity exists even if the D band does not. The Raman spectra of graphene has been used as a fingerprint of the number of layers using the G band position and I(G)/I(2D) ratio (35−37) and more recently through the 2D band position and shape (11). The intensity of the D band also correlates to defect density (11).

The observed Raman spectra of the pristine fiber spectrum (i) in Figure 3a with an I(D)/I(G) ratio of 0.084 is consistent with those observed from similar carbon fibers

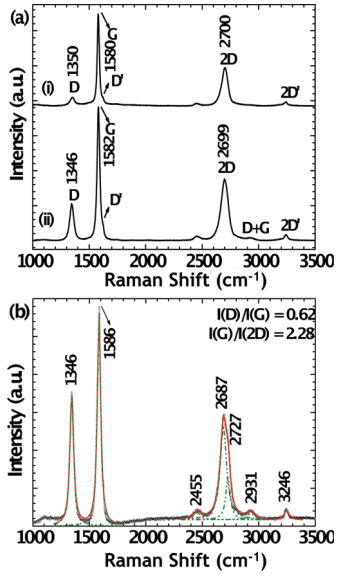

FIGURE 3. (a) Raman spectra of carbon fiber (i) before growth and (ii) after 30 min of growth duration showing few layers of graphene. (b) Raman spectra obtained after subtracting the two spectra in a, namely, ii − i.

(38, 39) and suggests that the carbon fibers are not fully graphitized (39). The Raman spectrum from the decorated fiber, shown in the lower spectrum (ii) of Figure 3a, is dominated by three strong bands (along with the other weak expected bands): D band at 1346 cm^{-1}, G band at 1582 cm^{-1}, and 2D band at 2700 cm^{-1}. The I(D)/I(G) ratio increased markedly to 0.28 after petal growth, and this ratio is similar to that reported for few-layer graphene (FLG) grown by plasma enhanced CVD techniques with I(D)/I(G) ratios between 0.2 and 0.3 (17, 23). The enhanced D band intensity is likely the result of defects arising from crack formation in graphene layers due to differences in substrate adhesion; these cracks then serve as sites for additional growth and folding of the graphene sheets. Also, increases in the 2D band's width and its intensity relative to the G band upon petal decoration are consistent the formation of FLG (11).

Given that the Raman spectra in Figure 3a are generally similar and that the lower spectrum (ii) is a convolution of both underlying carbon fiber and its surface, we have subtracted the two curves, and the result is shown in Figure 3b. The feature in the region near 2700 cm^{-1} becomes more clearly the convolution of two underlying peaks at 2687 and 2727 cm^{-1}, and is consistent with profiles of FLG flakes between 5 and 25 layers (11). The TEM images in Figure 2 reveal a diversity of petal thicknesses that are expected to produce a similar composite Raman signature in this region. Further the I(D)/I(G) and I(G)/I(2D) ratios suggest the presence of a FLG with large defect density, but the values are very similar to those produced by plasma PECVD techniques (17, 23).

X-ray photoelectron spectroscopy (XPS) analysis was performed to determine the different forms of carbon species. Figure 4 shows the core level C(1s) spectra recorded for the fibers before and after the growth. The shape peak (Figure 4a) at 284.6 eV corresponds to C═C graphitic species as reported (40). The spectrum after the growth process

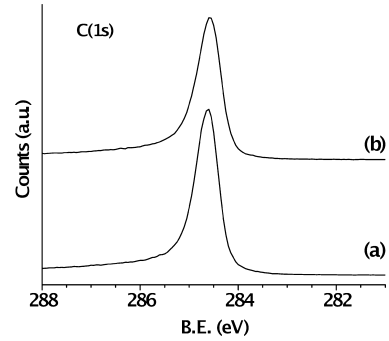

FIGURE 4. X-ray photoelectron core level C(1s) spectra of carbon fiber (a) before and (b) after 30 min of growth duration.

looks quite similar to the pristine fiber itself, with a shape peak at 284.6 eV with no peaks at higher binding energies. Peaks due to C−O species (286.6 eV), C═O species (287.9 eV), or the defect sp^3 C−C species (286.6 eV) are clearly absent (41, 42) indicating the purity of the grown flakes. The core level spectra recorded for oxygen (data not presented) is also quite similar, indicating that the introduction of oxygen for pretreatment and during the growth does not affect the quality of the graphitic species. Similar to Raman measurements, XPS analysis also supports the carbon nanosheets outgrowth to be graphitic species and devoid of sp^3 species.

CONCLUSION

In conclusion, we report the growth of contiguous petals from graphite fibers by microwave plasma CVD without the use of catalyst. Atomic-scale imaging reveals continuity of graphene planes in the transition region from fiber to petal, suggesting that the outgrowths should exhibit good mechanical integrity and transport at interfaces. Important contributors to this result appear to include electric field enhancement in the plasma growth environment and the addition of a trace amount of oxygen to the gas mixture. Studies are ongoing to discern and optimize the associated thermochemical processes. The structures reported herein may find applications in composite materials for structural and/or thermal enhancement, fluid filters, suspended graphene films between fibers for new electronic device structures, efficient electron emitters, and biological or chemical electrodes.

Acknowledgment. T.B. thanks the Indo-US Science and Technology Forum for support (Award 115-2008/2009-10) and Purdue's Birck Nanotechnology Center's support from its Kirk Recharge Grant program; A.S. thanks the International Association for the Exchange of Students for Technical Experience for support under its summer internship program. The XPS data were obtained by the Surface Analysis Laboratory of the Birck Nanotechnology Center, Purdue University. The authors thank Prof. R. G. Reifenberger, G. Prakash, and Dr. A. Voevodin for informative discussions.

Supporting Information Available: Details of synthesis and characterization tools employed; AFM data along with SEM images of growth near the tip of the fiber and on other

carbon substrates (PDF). This material is available free of charge via the Internet at http://pubs.acs.org.

REFERENCES AND NOTES

(1) Baughman, R. H.; Zakhidov, A. A.; de Heer, W. A. *Science* **2002**, *297*, 787–792.
(2) Geim, A. K.; Novoselov, K. S. *Nat. Mater.* **2007**, *6*, 183–191.
(3) Avouris, P.; Chen, Z.; Perebeinos, V. *Nat. Nanotechnol.* **2007**, *2*, 605–615.
(4) Cola, B. A.; Xu, J.; Cheng, C. R.; Xu, X. F.; Fisher, T. S.; Hu, H. P. *J. Appl. Phys.* **2007**, *101*, 054313–9.
(5) Prasher, R.; Tong, T.; Majumdar, A. *J. Appl. Phys.* **2007**, *102*, 104312–10.
(6) Hughes, J. D. H. *Compos. Sci. Technol.* **1991**, *41*, 13–45.
(7) Rao, C. N. R.; Sood, A. K.; Subrahmanyam, K. S.; Govindaraj, A. *Angew. Chem., Int. Ed.* **2009**, *48*, 7752–7777.
(8) Prasada, K. E.; Das, B.; Maitra, U.; Ramamurty, U.; Rao, C. N. R. *Proc. Natl. Acad. Sci. U.S.A.* **2009**, *106*, 13186–13189.
(9) Chen, Z.; Lin, Y.; Rooks, M.; Avouris, P. *Phys. E* **2007**, *40*, 228–232.
(10) Das, A.; Pisana, S.; Chakraborty, B.; Piscanec, S.; Saha, S. K.; Waghmare, U. V.; Novoselov, K. S.; Krishnamurthy, H. R.; Geim, A. K.; Ferrari, A. C.; Sood, A. K. *Nat. Nanotechnol.* **2008**, *3*, 210–215.
(11) Das, A.; Chakraborty, B.; Sood, A. *Bull. Mater. Sci.* **2008**, *31*, 579–584.
(12) Wang, G.; Yang, J.; Park, J.; Gou, X.; Wang, B.; Liu, H.; Yao, J. *J. Phys. Chem. C* **2008**, *112*, 8192–8195.
(13) Amama, P. B.; Maschmann, M. R.; Fisher, T. S.; Sands, T. D. *J. Phys. Chem. B* **2006**, *110*, 10636–10644.
(14) Zhu, M.; Wang, J.; Holloway, B. C.; Outlaw, R. A.; Zhao, X.; Hou, K.; Shutthanandan, V.; Manos, D. M. *Carbon* **2007**, *45*, 2229–2234.
(15) Wu, Y.; Qiao, P.; Chong, T.; Shen, Z. *Adv. Mater.* **2002**, *14*, 64–67.
(16) Geis, M. W.; Twichell, J. C.; Lyszczarz, T. M. *J. Vac. Sci. Technol., B* **1996**, *14*, 2060–2067.
(17) Wang, J.; Zhu, M.; Outlaw, R. A.; Zhao, X.; Manos, D. M.; Holloway, B. C. *Carbon* **2004**, *42*, 2867–2872.
(18) Yuan, G. D.; Zhang, W. J.; Yang, Y.; Tang, Y. B.; Li, Y. Q.; Wang, J. X.; Meng, X. M.; He, Z. B.; Wu, C. M. L.; Bello, I.; Lee, C. S.; Lee, S. T. *Chem. Phys. Lett.* **2009**, *467*, 361–364.
(19) Ando, Y.; Zhao, X.; Ohkohchi, M. *Carbon* **1997**, *35*, 153–158.
(20) Subrahmanyam, K. S.; Panchakarla, L. S.; Govindaraj, A.; Rao, C. N. R. *J. Phys. Chem. C* **2009**, *113*, 4257–4259.
(21) Sreekumar, T. V.; Liu, T. B.; Min, G.; Guo, H.; Kumar, S.; Hauge, R. H.; Smalley, R. E. *Adv. Mater.* **2004**, *16*, 58–61.
(22) Veca, L. M.; Meziani, M. J.; Wang, W.; Wang, X.; Lu, F.; Zhang, P.; Lin, Y.; Fee, R.; Connell, J. W.; Sun, Y.-P. *Adv. Mater.* **2009**, *21*, 2088–2092.
(23) Malesevic, A.; Vitchev, R.; Schouteden, K.; Volodin, A.; Zhang, L.; Tendeloo, G. V.; Vanhulsel, A.; Haesendonck, C. V. *Nanotechnology* **2008**, *19*, 305604.
(24) Ruland, W. *Adv. Mater.* **1990**, *2*, 528–536.
(25) Gupta, A. K.; Paliwal, D. K.; Bajaj, P. J. *Macromol. Sci.* **1991**, *C31*, 1–89.
(26) Wightman, J.; DeVilbiss T.; Dillard, J. In *International Encyclopedia of Composites* Lee, S., Ed.; VCH Publishers: New York, 1990; p 226.
(27) Drzal, L. T.; Rich, M. J.; Lloyd, P. F. *J. Adhes.* **1982**, *16*, 1–30.
(28) Drzal, L. T.; Rich, M. J.; Koenig, M. F.; Lloyd, P. F. *J. Adhes.* **1983**, *16*, 133–152.
(29) Jang, B. Z. *Compos. Sci. Technol.* **1992**, *44*, 333–349.
(30) Dilsiz, N. *J. Adhes. Sci. Technol.* **2000**, *14*, 975–987.
(31) Petherbridge, J. R.; May, P. W.; Ashfold, M. N. R. *J. Appl. Phys.* **2001**, *89*, 5219–5223.
(32) Garg, R. K.; Kim, S. S.; Hash, D. B.; Gore, J. P.; Fisher, T. S. *J. Nanosci. Nanotechnol.* **2008**, *8*, 3068–3076.
(33) Cola, B. A.; Karru, R.; Cheng, C. R.; Xu, X. F.; Fisher, T. S. *IEEE Trans, Compon., Packag., Technol.* **2008**, *31*, 46–53.
(34) Kumar, G. V. P.; Narayana, C. *Curr. Sci.* **2007**, *93*, 778–781.
(35) Ferrari, A. C.; Meyer, J. C.; Scardaci, V.; Casiraghi, C.; Lazzeri, M.; Mauri, F.; Piscanec, S.; Jiang, D.; Novoselov, K. S.; Roth, S.; Geim, A. K. *Phys. Rev. Lett.* **2006**, *97*, 187401–4.
(36) Gupta, A.; Chen, G.; Joshi, P.; Tadigadapa, S.; Eklund, P. C. *Nano Lett.* **2006**, *6*, 2667–2673.
(37) Graf, D.; Molitor, F.; Ensslin, K.; Stampfer, C.; Jungen, A.; Hierold, C.; Wirtz, L. *Nano Lett.* **2007**, *7*, 238–242.
(38) Knight, D. S.; White, W. B. *J. Mater. Res.* **1989**, *4*, 385–393.
(39) Fauteux, C.; Pegna, J. *Appl. Phys. A: Mater. Sci. Process.* **2004**, *78*, 883–888.
(40) Paredes, J. I.; Villar-Rodil, S.; Martínez-Alonso, A.; Tascon, J. M. D. *Langmuir* **2008**, *24*, 10560–10564.
(41) Yang, D.-Q.; Rochette, J.-F.; Sacher, E. *Langmuir* **2005**, *21*, 8539–8545.
(42) Yang, D.-Q.; Sacher, E. *Langmuir* **2006**, *22*, 860–862.

AM9009154